1. Introduction and Motivation

The electromagnetic response functions for the transition of a proton to its excited states reflect the quark wavefunctions of the initial and final hadronic states and the transition operator connecting them. This information is experimentally accessible through the determination of the multipole components of the transition.

In the SU(6) spherically symmetric quark model, the nucleon and Δ have all three quarks in an overall S-state $(1s)^3$. While such spherically symmetric wavefunctions enjoyed numerous successes, they were, however, unable to reproduce the observed values of the axial-to-vector-coupling-constant ratio g_A/g_V, the SU(3) decay ratio (D+F)/(D-F) and the ratio of the pion-nucleon-Δ to the pion-nucleon-nucleon coupling constants $G_{\pi N\Delta}/G_{\pi NN}$. Glashow[1] and then Vento, Baym and Jackson[2] showed that these problems can be resolved if a significant ($\sim$ 25%) D-state admixture were present in the nucleon and isobar wavefunctions. The non-zero neutron charge radius is also evidence for non-sphericity in the 3-quark wavefunctions[3] Furthermore, D-state admixtures are relevant for the deep inelastic spin structure functions.[4][5] Writing the nucleon wavefunction as:

$$|N\rangle = \sqrt{1-P_D}|56,0^+\rangle + \sqrt{P_D}|70,2^+\rangle \quad , \tag{1}$$

Abbas[5] showed that, in the context of the constituent quark model, the integrals of the spin structure functions are:

$$\int_0^1 g_1^p(x)\,dx = \frac{15-24P_D}{54}, \qquad \int_0^1 g_1^n(x)\,dx = -\frac{P_D}{9} \quad . \tag{2}$$

A value of $P_D \approx 0.3$ would be consistent with the EMC,[6] SMC[7] and E142[8] results. While it is obviously naive to ascribe sole responsibility for the results to this single parameter, it is equally obvious that the role of quark orbital angular momentum must be understood to properly interpret the spin structure functions.

The microscopic origin of such a deformation is explained in different ways by different nucleon models. The Chiral Bag Model[9] explains the deformation as due to the different pressure that the pion cloud exerts on the bag along the spin direction and in directions normal to it. In the Constituent Quark Model[10] the S-D wave mixing arises from the color hyperfine interaction[11] derived from a non-relativistic reduction of the one-gluon-exchange potential and consists of a spin-spin and a tensor term. Relativistic Quark Models,[12] due to relativistic invariance alone, even without the hyperfine interaction, produce nonspherical components in the N and Δ wavefunctions.

The $N \rightarrow \Delta$ transition provides an excellent opportunity to investigate the $\ell = 2$ admixture since, for spherically symmetric wavefunctions, the electromagnetic quadrupole amplitudes S_{1+} and E_{1+} (or C2 and E2) would have to vanish even though they are allowed by the selection rules. The experimental challenge is isolating these multipoles in the presence of the dominant magnetic dipole M_{1+} (or M1) amplitude.

Extensive electromagnetic studies of the Δ were carried out during the sixties and seventies and data from DESY [13] and NINA[14] on neutral pion production already have shown the inconsistency of the data with a pure magnetic dipole transition since such a transition would require the following relation between the Legendre coefficients in the

Figure 1. *Angular coefficients versus invariant mass for neutral pion electroproduction.*[13][14]. *The curves are a dispersion theory calculation of von Gehlen.*[15]

angular distribution:

$$\frac{\bar{A}_0}{\bar{A}_2} = -\frac{5}{3}, \quad \bar{A}_0 = C_0, \quad \bar{A}_1 = D_1 = D_0 = 0 \quad . \tag{3}$$

As can be seen in Figure 1, this is clearly not the case.

The current experimental knowledge of the quadrupole amplitudes is, however, unsatisfactory, resulting from unpolarized experiments[13][14] carried out with low duty cycle and low intensity beams which resulted in a limited number of structure functions often extracted with large uncertainties. Figure 2 displays the extracted Coulomb and electric quadrupole terms along with the predictions of various models: the results of the dispersion relation analysis of Devenish and Lyth[16] (DL), non-relativistic quark models (NRQM)[17][18] a relativized quark model[19], and the Generalized Vector Dominance Model.[20]

The complete determination of the multipole components in a transition is hindered when (some of) the components are relatively small and when non-resonant background or tails of other resonances are present. CEBAF holds the promise of a significant improvement in determining resonance parameters by the exploitation of polarization observables. The advantage of such polarization studies is, of course, that many of these observables result from interferences between a large and a small amplitude, making the observable linear in the small amplitude and, consequently, its determination considerably easier than from an unpolarized measurement where it would occur quadratically. Furthermore, the limited number of observables (four) in unpolarized measurements exacerbates the extraction of individual resonance parameters; what is needed in addition to better unpolarized measurements is an increased number of observables. This requires exploiting the polarization degrees of freedom.

Many of the amplitudes accessible by polarization measurements in the electron scattering plane either do not occur in unpolarized experiments or require out-of-plane measure-

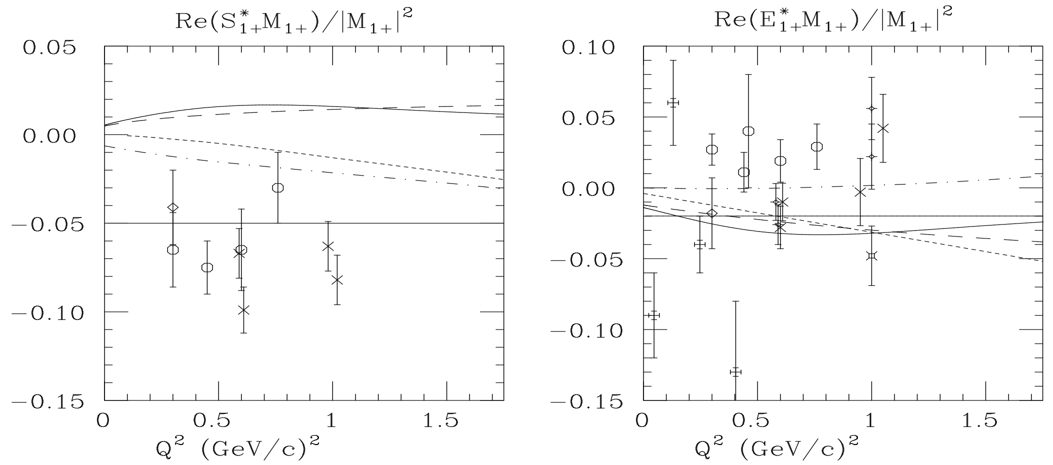

Figure 2. *Theoretical predictions for the S_{1+} and E_{1+} multipole amplitudes compared to previous data.*[13][14] *Solid and long-dashes: relativistic and non-relativistic quark models from ref.*[19] *short-dash: NRQM of ref.*[18] *and dot-dash: Generalized Vector Dominance Model calculation from ref.*[20]*. The horizontal lines at* -0.05 *and* -0.02 *indicate the fixed values of S_{1+} and E_{1+} respectively in the DL*[16] *parameterization.*

ments for their determination. In fact, unpolarized experiments, even with out-of-plane coverage, only determine the real parts of interference amplitudes; polarization, either of the electron beam, the recoil proton, or both, must be invoked to probe the imaginary parts. These have the feature of vanishing identically if the final state is determined by a single phase, as it would be for a single isolated resonance. Thus, these imaginary pieces are especially important since, when studying a given resonance, they will allow the contribution from other resonances and non-resonant terms to be characterized.

This proposal addresses response function separations of the $\mathrm{p}(\vec{\mathrm{e}},\mathrm{e}'\vec{\mathrm{p}})\pi^0$ reaction. The measurements we propose are complementary to the studies planned for CLAS. On the one hand, the recoil polarization observables are composed of different combinations of amplitudes than the polarized target ones. Of equal importance is that in Hall A, the precise definition of the kinematics on an event-by-event basis will enable us to perform separations of individual response functions to high accuracy. This precise determination of absolute response functions, combined with the extensive angular distribution[21] and asymmetry[22] [23] [24] data from CLAS, will result in a considerably deeper knowledge of hadronic structure.

1.1 Relation to Previous Proposal

This updated proposal differs considerably from the previous, conditionally approved version. We have addressed all the issues raised by PAC5. The major changes are:

- The proposal has been restricted in scope to study only the Δ resonance.
- Measurement of more angular points at a fixed Q^2 to allow a multipole analysis. The statistical precision is lower than originally proposed but many more angles

are measured. This will yield more useful information than measuring a small number of angles and several Q^2 points. In particular, it allows a "stand-alone" multipole analysis of this data by itself.

- Emphasis of the LT-type response functions since the Hall A-FPP combination is unique in its ability to extract nearly the maximal amount of information regarding the $\mathrm{Re}(S_{1+}^* M_{1+})$ interference term.
- The kinematics chosen correspond to ones approved for CLAS.
- Exploitation of the fairly large acceptance in W to obtain data below, on and above the Δ resonance. Specifically, data will be taken at resonance ($W = 1.232$ GeV) and 40 MeV above and below resonance.

2. Coincident Pion Electroproduction

The formalism for the $\mathrm{p}(\vec{\mathrm{e}},\mathrm{e}'\vec{\mathrm{p}})\pi^0$ reaction has been developed by Donnelly and Raskin[25] and recently employed to explore the sensitivity of the recoil proton polarization to representative models of pion electroproduction.[26][27] The cross section for this reaction has the form:[28]

$$\frac{d^3\sigma}{de'd\Omega_{e'}d\Omega_p^*} = \sigma_0 \frac{1}{2}\left[1 + \vec{P}\cdot\vec{\sigma} + h(A + \vec{P}'\cdot\vec{\sigma})\right] \quad , \tag{4}$$

where σ_0 is the unpolarized cross section, $\vec{P}$ is the induced polarization, A is the electron analyzing power and $\vec{P}'$ are the spin transfer coefficients (h is the helicity of the incident electron). The proton polarization $\vec{\Pi}$ thus consists of two pieces: $\vec{\Pi} = \vec{P} + h\vec{P}'$. In more detail, the cross section contains eighteen response functions.[29] Here it is given in the form often used for electroproduction, differential in LAB electron variables and center-of-mass (CM) hadron ones:[25]

$$\begin{aligned}\frac{d^3\sigma}{de'd\Omega_{e'}d\Omega_p^*} =& \Gamma_t \frac{p_p^* W}{K_\gamma M_p}\Big\{2\varepsilon_L\left(R_L + R_L^n\mathcal{S}_n\right) + \left(R_T + R_T^n\mathcal{S}_n\right) \\ & -\varepsilon\left[\left(R_{TT} + R_{TT}^n\mathcal{S}_n\right)\cos 2\phi + \left(R_{TT}^\ell\mathcal{S}_l + R_{TT}^t\mathcal{S}_t\right)\sin 2\phi\right] \\ & -\sqrt{\varepsilon_L(1+\varepsilon)}\left[\left(R_{LT} + R_{LT}^n\mathcal{S}_n\right)\cos\phi + \left(R_{LT}^\ell\mathcal{S}_l + R_{LT}^t\mathcal{S}_t\right)\sin\phi\right] \\ & -h\sqrt{\varepsilon_L(1-\varepsilon)}\left[\left(R'_{LT} + R'^{\,n}_{LT}\mathcal{S}_n\right)\sin\phi + \left(R'^{\,\ell}_{LT}\mathcal{S}_l + R'^{\,t}_{LT}\mathcal{S}_t\right)\cos\phi\right] \\ & +h\sqrt{1-\varepsilon^2}\left(R'^{\,\ell}_{TT}\mathcal{S}_l + R'^{\,t}_{TT}\mathcal{S}_t\right)\Big\}\end{aligned} \quad , \tag{5}$$

where the subscripts L, T, LT and TT denote longitudinal, transverse, longitudinal-transverse interference and transverse-transverse interference terms respectively (the prime ($'$) denotes those response functions which require polarized electrons). The proton mass is M_p, W is the invariant mass of the hadronic final state, Γ_t is the virtual photon flux, $K_\gamma = (W^2 - M_p^2)/2W$, p_p^* is the proton three-momentum in the CM,

$$\varepsilon^{-1} \equiv 1 + \frac{2q^2}{Q^2}\tan^2\theta_e/2 \quad , \tag{6}$$

is the longitudinal polarization of the virtual photon, $\varepsilon_L = \varepsilon(Q^2/(q^*)^2)$ and $q^*(q)$ is the three-momentum transfer in the CM (LAB). The projections of the proton spin vector are given by: $\mathcal{S}_n = \hat{n}\cdot\hat{s}'_R$, $\mathcal{S}_l = \hat{l}\cdot\hat{s}'_R$, $\mathcal{S}_t = \hat{t}\cdot\hat{s}'_R$, and $\hat{s}'_R$ is the spin vector in the proton rest frame. The coordinate system has $\hat{\ell}$ along the proton momentum, $\hat{n}$ normal to the reaction plane and $\hat{t} = \hat{n}\times\hat{\ell}$. Finally, ϕ is the angle between the (e,e$'$) plane and the plane containing $\vec{q}$ and $\vec{p_p}^*$.

We are only concerned with measurements in the (e,e$'$) plane. Then the components of $\vec{\Pi} = (\Pi_n, \Pi_t, \Pi_\ell)$ are:

$$\begin{aligned}
\tilde{\sigma}_0 \Pi_n &= 2\varepsilon R_L^n + R_T^n - \varepsilon R_{TT}^n \mp \sqrt{\varepsilon_L(1+\varepsilon)} R_{LT}^n \\
\tilde{\sigma}_0 \Pi_t &= h\left(\sqrt{1-\varepsilon^2} R'^{\,t}_{TT} \mp \sqrt{\varepsilon_L(1-\varepsilon)} R'^{\,t}_{LT}\right) \\
\tilde{\sigma}_0 \Pi_\ell &= h\left(\sqrt{1-\varepsilon^2} R'^{\,\ell}_{TT} \mp \sqrt{\varepsilon_L(1-\varepsilon)} R'^{\,\ell}_{LT}\right) \quad ,
\end{aligned} \tag{7}$$

where $\tilde{\sigma}_0$ is the unpolarized cross section except for σ_{Mott}:

$$\tilde{\sigma}_0 = 2\varepsilon_L R_L + R_T - \varepsilon R_{TT} \mp \sqrt{\varepsilon_L(1+\varepsilon)} R_{LT} \quad , \tag{8}$$

and the upper(lower) sign refers to $\phi = 0°(180°)$. We will perform measurements on either side of $\vec{q}$ so that the terms on either side of the $\pm$ can be separated. Furthermore, in the case of parallel kinematics ($\vec{q} \parallel \vec{p}\,'$) the components of the proton polarization reduce to:

$$\begin{aligned}
\Pi_n &= \frac{1}{\tilde{\sigma}_0}\left\{\sqrt{\varepsilon_L(1+\varepsilon)} R_{LT}^n\right\} \\
\Pi_t &= \frac{1}{\tilde{\sigma}_0}\left\{h\sqrt{\varepsilon_L(1-\varepsilon)} R'^{\,t}_{LT}\right\} \\
\Pi_\ell &= \frac{1}{\tilde{\sigma}_0}\left\{h\sqrt{1-\varepsilon^2} R'^{\,\ell}_{TT}\right\} \quad .
\end{aligned} \tag{9}$$

A multipole representation allows one to consider the resonant and the (equally important) non-resonant terms separately. In the specific case of pion electroproduction at the Δ resonance, and assuming that 1) only s- and p-waves contribute and 2) that terms which do not contain the (large) M_{1+} amplitude are negligible, then the following explicit multipole decomposition of the response functions separable by in-plane measurements results:[25]

$$\begin{aligned}
R'^{\,\ell}_{TT} &= \frac{5}{3}|M_{1+}|^2 - 2\mathrm{Re}\{E^*_{1+}M_{1+} + \frac{2}{3}M^*_{1-}M_{1+}\} + 2\mathrm{Re}\left\{E^*_{0+}M_{1+}\right\} P_1(\cos\theta_{cm}) \\
&\quad - \left(\frac{2}{3}|M_{1+}|^2 - \mathrm{Re}\{8E^*_{1+}M_{1+} + \frac{2}{3}M^*_{1-}M_{1+}\}\right) P_2(\cos\theta_{cm}) \quad , \\
R'^{\,t}_{TT} &= \sin\theta_{cm}\left(\mathrm{Re}\left\{E^*_{0+}M_{1+}\right\} + \left(|M_{1+}|^2 + \mathrm{Re}\left\{6M^*_{1+}E_{1+} + M^*_{1-}M_{1+}\right\}\right) P_1(\cos\theta_{cm})\right) \quad , \\
R'^{\,\ell}_{LT} &= -\sqrt{2}\sin\theta_{cm}\,\mathrm{Re}\left(2S^*_{0+}M_{1+} + \left\{S^*_{1-}M_{1+} + 10S^*_{1+}M_{1+}\right\} P_1(\cos\theta_{cm})\right) \quad , \\
R'^{\,t}_{LT} &= \sqrt{2}\,\mathrm{Re}\left(\frac{5}{3}S^*_{1-}M_{1+} - \frac{4}{3}S^*_{1+}M_{1+} + S^*_{0+}M_{1+}P_1(\cos\theta_{cm})\right. \\
&\quad \left. -\frac{2}{3}\left\{S^*_{1-}M_{1+} - 8S^*_{1+}M_{1+}\right\} P_2(\cos\theta_{cm})\right) \quad ,
\end{aligned} \tag{10}$$

$$R_{LT} = -\sqrt{2}\sin\theta_{cm}\,\mathrm{Re}\left(S^*_{0+}M_{1+} + 6S^*_{1+}M_{1+}P_1(\cos\theta_{cm})\right)$$

and

$$R^n_{LT} = -\sqrt{2}\,\mathrm{Im}\left(S^*_{1-}M_{1+} + S^*_{0+}M_{1+}P_1(\cos\theta_{cm}) + 4S^*_{1+}M_{1+}P_2(\cos\theta_{cm})\right) \quad ,$$

where θ_{cm} is the proton angle with respect to $\vec{q}$ in the $N\pi$ center of mass system. Note that the angular momentum algebra allows the response functions to written in terms of the first three Legendre polynomials, providing the means for the multipole analysis we will perform.

One feature of the response functions is especially important for the present proposal: $R'^{t}_{LT}, R'^{\ell}_{LT}$ and R_{LT} all contain the $\mathrm{Re}(S^*_{1+}M_{1+})$ interference term *and only one more of the remaining 15 response functions does. It, however, requires both polarimetry and out-of-plane capability for its determination.* In addition, none of these three response functions contain the large $|M_{1+}|^2$ term. The combination of a polarized electron beam and a proton polarimeter (or polarized target) allow the maximum amount of information on the $\mathrm{Re}(S^*_{1+}M_{1+})$ term to be extracted. Hall A is unique in being able to actually determine three of the four response since the polarized target proposal for CLAS[23] will only employ a single direction of target polarization (along the incident beam). Having three independent observables will, within the above approximations, allow us to both virtually isolate the S_{1+} term and determine the remaining (S_{1-} and S_{0+}) non-resonant longitudinal strength. Although in the absence of these approximations we can no longer unambiguously extract S_{1+}, the three LT-type observables still provide multiple redundancy and permits one to place much more stringent constraints on the scalar quadrupole contribution than can any single LT response alone.

A measure of the non-Δ contributions (Born terms and other resonances) is provided by the R^n_{LT} and $2\varepsilon R^n_L + R^n_T - \varepsilon R^n_{TT}$ response functions. Since they are the imaginary part of an interference, then, if only amplitudes from a single resonance are present (so that the final state is determined by a single phase) we would have these normal-polarized response functions $\equiv 0$.

3. Experimental Procedure

Our goal is to make a precise measurement of the $p(\vec{e},e'\vec{p})\pi^0$ reaction at the maximum of the Δ resonance and separate six individual response functions. These are: $R'^{\ell}_{LT}, R'^{t}_{LT}, R^n_{LT}, R_{LT}, R'^{\ell}_{TT}$ and R'^{t}_{TT}. Five of these are new, i.e., have never been measured. In addition, we will determine the combinations $2\varepsilon R^n_L + R^n_T - \varepsilon R^n_{TT}$ and $2\varepsilon R_L + R_T - \varepsilon R_{TT}$. A four-momentum transfer of 1.0 GeV^2 has been chosen. All measurements will have a virtual photon polarization $\varepsilon = 0.9$ to enhance the contribution of the LT-type responses. Complete kinematics are given in Table 1. The measurements will require an electron beam of 100μA intensity and 40% polarization. We will employ the two Hall A spectrometers, one of which will be equipped with a focal plane polarimeter, for detection of electrons and polarized protons. The above items are all part of the basic instrumentation of CEBAF and Hall A.

Kinematics

$$E_0 = 3.20 \text{ GeV}, \ \theta_e = 21.1^\circ, \theta_q = 39.2^\circ$$
$$Q^2 = 1.0 \text{ GeV}^2, \ W = 1.232 \text{ GeV}$$
$$|\vec{q}| = 1.33 \text{ GeV/c}, \ \omega = 0.87 \text{ GeV}$$

Kin	θ^{pq}_{cm} deg	θ^{pq}_{lab} deg	θ_p deg	ϕ deg	$\lvert\vec{P}_p\rvert$ GeV/c
1	0	0	39.2	N/A	1.38
2,3	30	4.9	34.3, 44.1	0, 180	1.34
4,5	50	7.9	31.3, 47.1	0, 180	1.27
6,7	70	10.5	28.7, 49.7	0, 180	1.18
8,9	120	12.7	26.5, 51.9	0, 180	0.89
10,11	140	10.5	28.7, 49.7	0, 180	0.80
12,13	160	6.1	33.1, 45.3	0, 180	0.73

Table 1. *Kinematics for the $p(\vec{e},e'\vec{p})\pi^0$ experiment. The angles with superscript 'pq' are with respect to the $\vec{q}$ direction while θ_p is with respect to the incident beam.*

The separation of the LT-type response functions requires measurements to be made on both sides of $\vec{q}$, corresponding to $\phi = 0^\circ$ and $\phi = 180^\circ$. We will make measurements at a total of 13 proton angles; one of them corresponds to parallel kinematics while the other 12 (six on each side of $\vec{q}$) will allow the separation of the polarized LT- and TT-type response functions along with the unpolarized R_{LT}. By making this set of measurements we will:

- Determine the three response functions R^n_{LT}, R'^{t}_{LT} and R'^{ℓ}_{TT} at seven values of θ_{cm};
- Determine the three response functions $R'^{t}_{TT}, R'^{\ell}_{LT}$ and R_{LT} at six values of θ_{cm};
- Determine the two combinations of response functions $2\varepsilon R^n_L + R^n_T - \varepsilon R^n_{TT}$ and $2\varepsilon_L R_L + R_T - \varepsilon R_{TT}$ at six values of θ_{cm};
- Determine the response function combination $2\varepsilon R_L + R_T$ at one value of θ_{cm}.

The proton momentum, which is completely correlated with angle, varies between 730 MeV/c at $\theta_{cm} = 160^\circ$ to 1380 MeV/c at $\theta_{cm} = 0$. The kinematics we will cover are displayed in Figure 3 where the motivation for the choice of angles may also be discerned: we avoid working in the vicinity of the maximum lab angle since this corresponds to a broad range of center-of-mass angles. We also note that the protons from the $\Delta \rightarrow p\gamma$ decay are 5–6% higher in energy and could easily be resolved or excluded from the acceptance although in practice they present negligible contamination due to the 0.5% branching ratio to this channel.

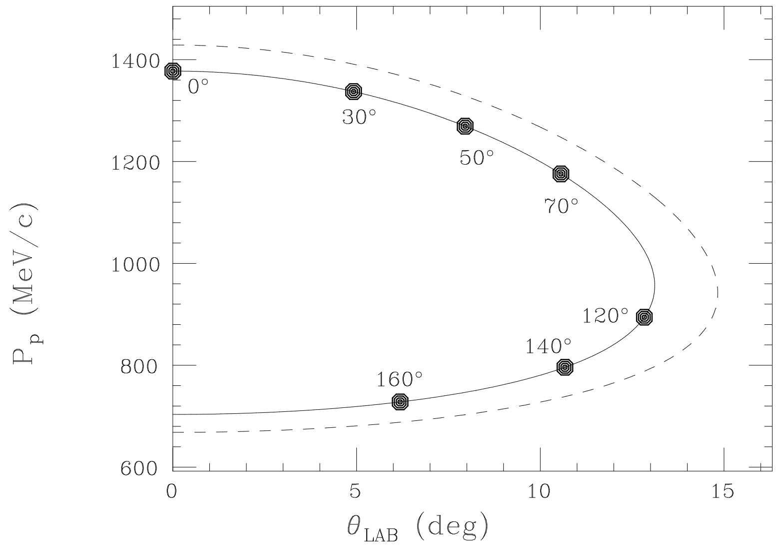

Figure 3. *Correlation of proton momentum with laboratory angle at $W = 1.232$ GeV and $Q^2 = 1.0$ GeV^2. The solid symbols indicate the proposed kinematic points labelled with the corresponding CM angles. The dashed line represents the kinematics of $\Delta \rightarrow p\gamma$.*

We will take advantage of the fact that Π_n is independent of the electron helicity to determine all three polarization components of the proton polarization even though the FPP only responds to two of the polarization components ($\hat{t}$ and $\hat{n}$). To see this, write the scattered intensity in the polarimeter as:

$$\begin{aligned} I(\theta,\phi) &= I_0(\theta)\big[1 + \Pi_n^{fp} A_y(\theta)\cos\phi + \Pi_t^{fp}(h) A_y(\theta)\sin\phi\big] \\ &= I_0(\theta)\big[1 + (\Pi_n^{tgt}\cos\chi + \Pi_\ell^{tgt}(h)\sin\chi) A_y(\theta)\cos\phi + \Pi_t^{tgt}(h) A_y(\theta)\sin\phi\big] \quad , \end{aligned} \tag{11}$$

where χ is the precession angle of the proton spin. Then, by making measurements with $\pm h$, we can separate the normal and longitudinal components of the target polarization vector:

$$\begin{aligned} \Pi_n^{tgt} &= \frac{\Pi_n^{fp}(+h) + \Pi_n^{fp}(-h)}{2\cos\chi} \\ \Pi_\ell^{tgt} &= \frac{\Pi_n^{fp}(+h) - \Pi_n^{fp}(-h)}{2\sin\chi} \quad . \end{aligned} \tag{12}$$

This technique is applicable as long as there is sufficient precession in the spectrometer magnets to produce appreciable $\hat{n}$-$\hat{\ell}$ mixing. Then the electron helicity can be used to flip the sign of the $\hat{\ell}$ component without affecting $\hat{n}$, thus allowing these two components to be separated. We will also utilize the techniques for polarimetry analysis developed by Ohlsen and co-workers at Los Alamos[30] that allow cancellation of instrumental asymmetries, detector efficiencies, solid angles and relative counting times by means of (somewhat involved) ratio methods.

3.1 Sensitivity of Proposed Measurement

The central physics issue in the $N \rightarrow \Delta$ transition is the presence, or absence, of quadrupole amplitudes. We have investigated the sensitivity of the polarization observables to such resonant quadrupole terms. The model for the Δ amplitudes was the dispersion relation based parameterization of Devenish and Lyth.[16] The higher nucleon resonances were also included according to the DL parameterization. We note that their longitudinal quadrupole amplitude is very similar to the one recently calculated by Laget.[31] To study the effects of the non-resonant Born (nucleon pole) terms we employed the calculation by von Gehlen.[32] These terms contain no imaginary parts. There seems to be a need for even more non-resonant terms, typically introduced phenomenologically,[33] so that the model calculations here represent a lower limit.

Representative results for all of the LT-type response functions are shown in Figure 4. The projected statistical error bars from this experiment are shown for the case with $S_{1+}/M_{1+} = -5\%$ and $E_{1+}/M_{1+} = -2\%$, i.e., as parameterized by DL. (Note that some models, in particular, Weber's,[34] indicate a considerably larger E_{1+} component which, if correct, would result in even higher sensitivity. Also, this model not only cures the longstanding problem in non-relativistic quark models of underestimating the low Q^2 M1 component but also describes that data well up to $Q^2 = 3$ GeV^2.) Statistical uncertainties range from 2–3% for the most favorable cases to 10–20% for the smaller polarization components. Systematic errors are expected to be below 5% (see below). The relatively low efficiency of the polarimeter means that we will obtain superb statistics for the unpolarized responses R_{LT} and $2\varepsilon R_L + R_T - \varepsilon R_{TT}$). The projected uncertainties in all the response functions are listed in Table 2.

We will also obtain good quality measurements of the quantities $2\varepsilon R_L + R_T - \varepsilon R_{TT}$ and $2\varepsilon R_L^n + R_T^n - \varepsilon R_{TT}^n$ with $\varepsilon = 0.90$. The unpolarized terms are dominated by $|M_{1+}|^2$, giving an independent determination of that quantity. Explicitly:

$$\begin{aligned} R_T &= 2|M_{1+}|^2 + 2\mathrm{Re}(E_{0+}^* M_{1+}) P_1(\cos\theta_{cm}) \\ &\quad - \left\{|M_{1+}|^2 + 2\mathrm{Re}(M_{1-}^* M_{1+} - 3E_{1+}^* M_{1+})\right\} P_2(\cos\theta_{cm}) \quad , \\ R_{TT} &= 3\sin^2\theta_{cm} \left\{\frac{1}{2}|M_{1+}|^2 + \mathrm{Re}(M_{1-}^* M_{1+} + E_{1+}^* M_{1+})\right\} \quad , \end{aligned} \tag{13}$$

(R_L is $\approx$ negligible since it is quadratic in the small scalar amplitudes). Since $R_{TT} = 0$ in parallel kinematics, we will essentially isolate R_T at that one point. Since we also separate the two TT-type polarized response functions, R'^{ℓ}_{TT} and R'^{t}_{TT}, we will have excellent consistency checks on $|M_{1+}|^2$. The projected results for these two responses is shown in Figure 5.

The normal-polarized terms are all imaginary parts of interferences:

$$\begin{aligned} R_L^n &= \sin\theta_{cm} \left\{\mathrm{Im}\left(S_{0+}^*(2S_{1+} - S_{1-})\right) + 6\,\mathrm{Im}(S_{1-}^* S_{1+}) P_1(\cos\theta_{cm})\right\} \quad , \\ R_T^n &= \sin\theta_{cm} \left\{\mathrm{Im}(E_{0+}^* M_{1+}) - 3\,\mathrm{Im}(M_{1-}^* M_{1+}) P_1(\cos\theta_{cm})\right\} \quad , \\ R_{TT}^n &= 3\sin\theta_{cm} \left\{\mathrm{Im}(E_{0+}^* M_{1+}) - \mathrm{Im}(M_{1-}^* M_{1+} - 4E_{1+}^* M_{1+}) P_1(\cos\theta_{cm})\right\} \quad . \end{aligned} \tag{14}$$

In the model we have employed, this sum of terms tends to be dominated by the $M_{1-}^* M_{1+}$ interference. We will achieve 5-25% statistical uncertainty on $2\varepsilon R_L^n + R_T^n - \varepsilon R_{TT}^n$ at all

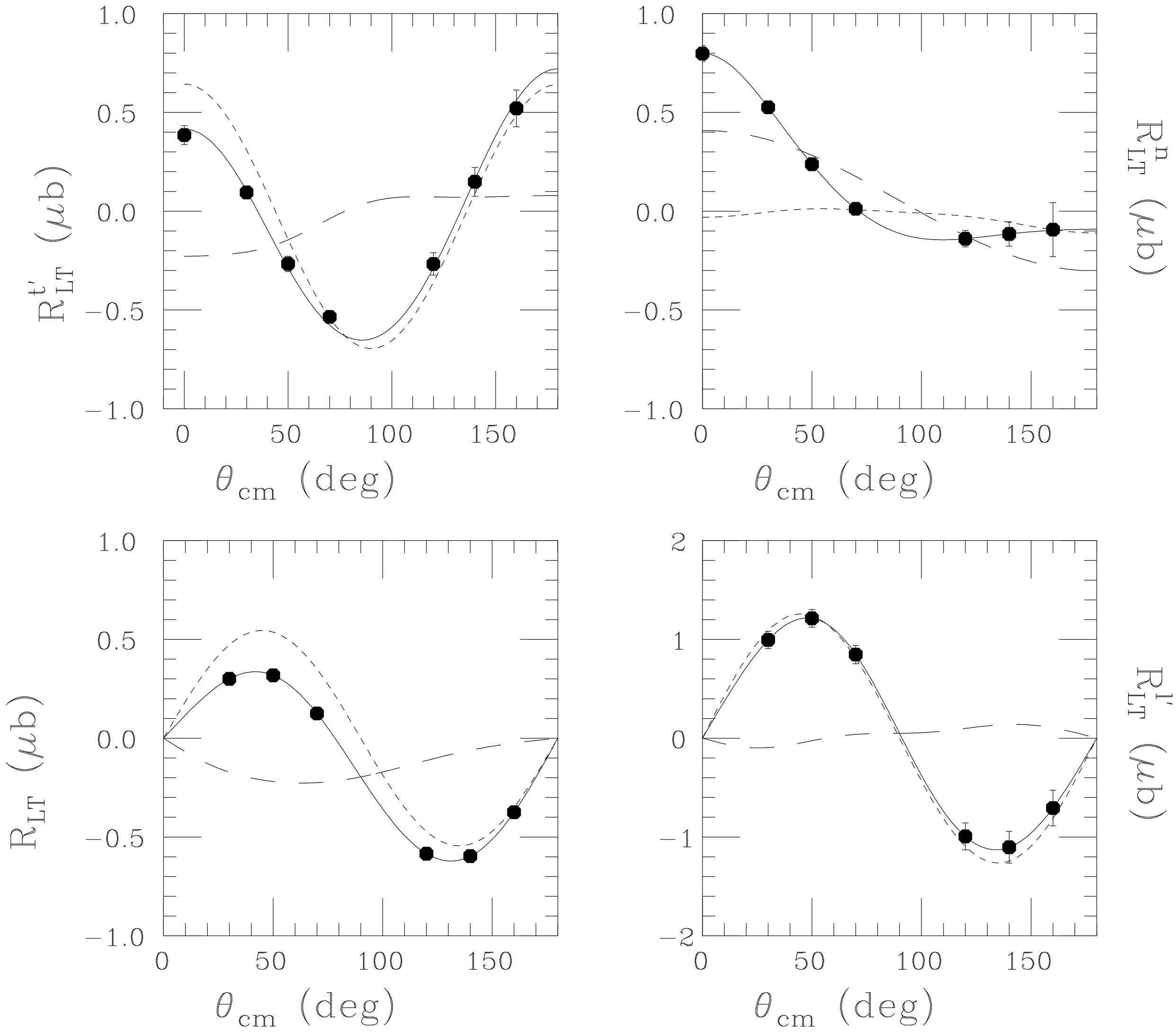

Figure 4. *Response functions $R_{LT}, R^n_{LT}, R'^{\ell}_{LT}$ and R'^{t}_{LT} for electroproduction at $W = 1.232$ GeV and $Q^2 = 1.0$ GeV^2. The error bars are the projected result of the experiment proposed here. Solid curve: full calculation according to DL parameterization. Long-dashed curve: S_{1+} and E_{1+} multipoles set to zero. Short-dashed curve: Born terms set to zero.*

but one point. The projected results are indicated in Figure 6. This sum of responses, like R^n_{LT} shown in Figure 4, is highly sensitive to the non-resonant terms.

3.2 W-Dependence

It is necessary to investigate the W-dependence of the response functions in order to best characterize the resonant contributions. The large values of final state momenta and the 10% acceptance of the Hall A spectrometers result in a W acceptance of over 150 MeV. This may be divided into at least 3 bins while maintaining reasonable statistics. This is adequate to detect the resonant variation with W as indicated in Figure 7 for two representative response functions (R^n_{LT} and R'^{t}_{LT}).

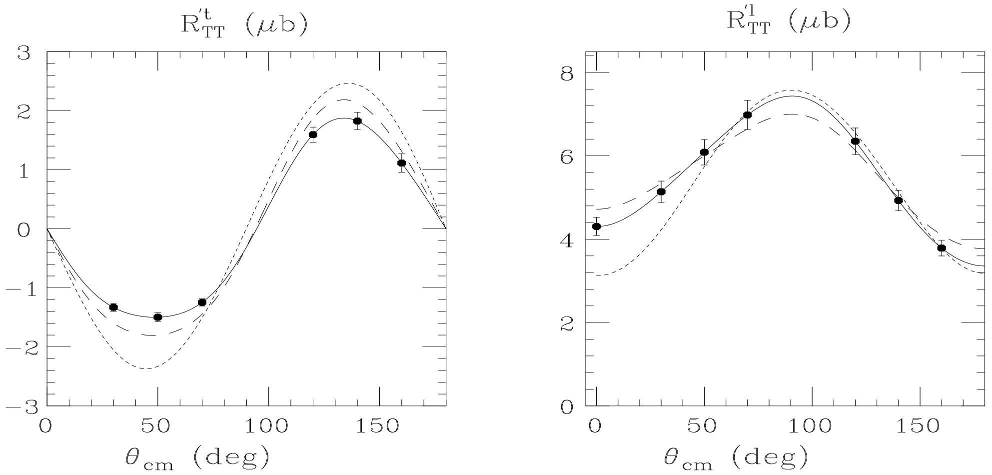

Figure 5. *TT-type response functions R'^{t}_{TT} and R'^{ℓ}_{TT} vs. θ_{cm} shown with projected statistical uncertainties. Solid curve: full calculation, long-dashed curve: $S_{1+} = E_{1+} = 0$, short-dashed curve: Born terms set to zero.*

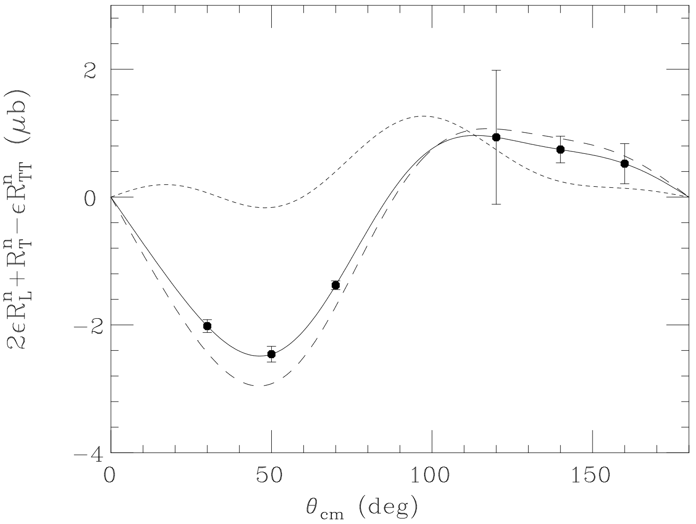

Figure 6. *Sum of normal-polarized response functions vs. θ_{cm}. Solid curve: full calculation, long-dashed curve: $S_{1+} = E_{1+} = 0$, short-dashed curve: Born terms set to zero.*

3.3 Multipole Analysis

This experiment will have sufficient angular coverage to permit a multipole analysis of the resulting response functions. In testing our ability to perform such an analysis, we considered a more extensive multipole content to the LT-type response functions than given in Eq. 10. In particular, we allowed for the presence of $S^*_{0+}M_{1+}$, $S^*_{0+}E_{0+}$, $S^*_{0+}M_{1-}$, $S^*_{1-}E_{0+}$, $S^*_{1-}M_{1+}$, $S^*_{1+}M_{1-}$ and $S^*_{1+}M_{1+}$ interference terms. These are known from earlier measurements to be the dominant contributions. We then fit each LT-type response function with a sum of Legendre polynomials up to $\ell = 4$. In addition to the statistical uncertainties listed in Table 2, we added a (conservative) $\pm 8\%$ systematic error to each data point. The response function pseudo-data were generated including all the

Projected Uncertainties

θ_{cm} (deg)	$R'^{\,t}_{TT}$	$R'^{\,t}_{LT}$	R^n_{LT}	$2\epsilon R^n_L + R^n_T$ $-\epsilon R^n_{TT}$	$R'^{\,\ell}_{TT}$	$R'^{\,\ell}_{LT}$	R_{LT}
0°	—	20	≤ 5	—	≤ 5	—	—
30°	≤ 5	18	≤ 5	≤ 5	≤ 5	9	≤ 5
50°	≤ 5	23	≤ 5	≤ 5	≤ 5	7	≤ 5
70°	≤ 5	9	24	≤ 5	≤ 5	11	≤ 5
120°	8	34	30	112	≤ 5	14	≤ 5
140°	8	78	54	28	≤ 5	15	≤ 5
160°	14	28	147	60	≤ 5	25	≤ 5

Table 2. *Projected statistical uncertainties (in percent) for the extracted response functions at each center-of-mass angle. Values below 5% are not quoted explicitly.*

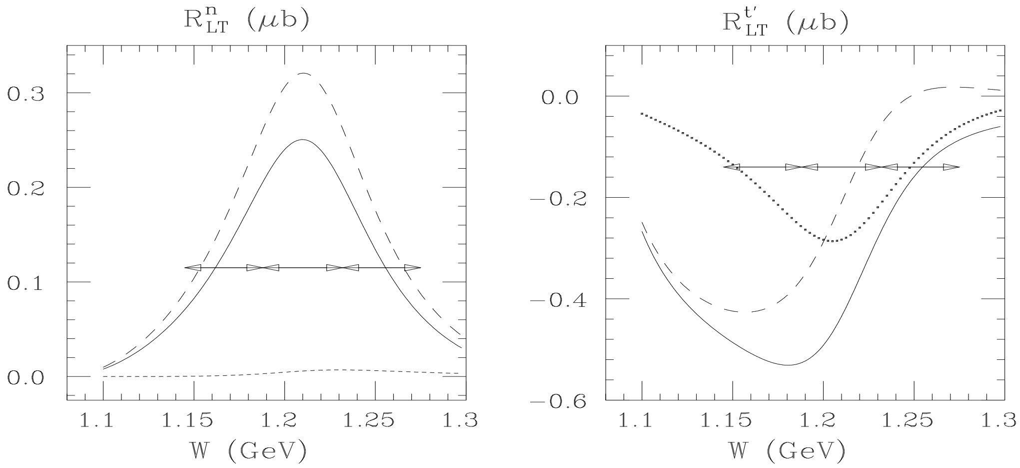

Figure 7. *The response functions R^n_{LT} and $R'^{\,t}_{LT}$ vs. invariant mass at $\theta_{cm} = 50°$. The arrows indicate the W acceptance of the Hall A spectrometers at this kinematics and three possible binnings. Solid curve: full calculation, long-dashed curve: $S_{1+} = E_{1+} = 0$, short-dashed curve: Born terms set to zero.*

higher resonances parameterized by Devenish and Lyth[16] viz. the $D_{13}(1520)$, $D_{15}(1675)$, $F_{15}(1688)$, $S_{31}(1620)$, $S_{11}(1700)$, $F_{37}(1950)$ and $G_{17}(2190)$. Born terms were included. The resulting fits are shown in Figure 8. We obtained $\mathrm{Re}(S^*_{1+}M_{1+}) = 0.168 \pm 0.010 \pm 0.013$ which is consistent with the input value of 0.179. Results of this quality would be a significant improvement in our knowledge of $\mathrm{Re}(S^*_{1+}M_{1+})$ as can be seen in Figure 9.

3.4 Systematic Errors

The are two primary sources of systematic errors: uncertainties associated with the

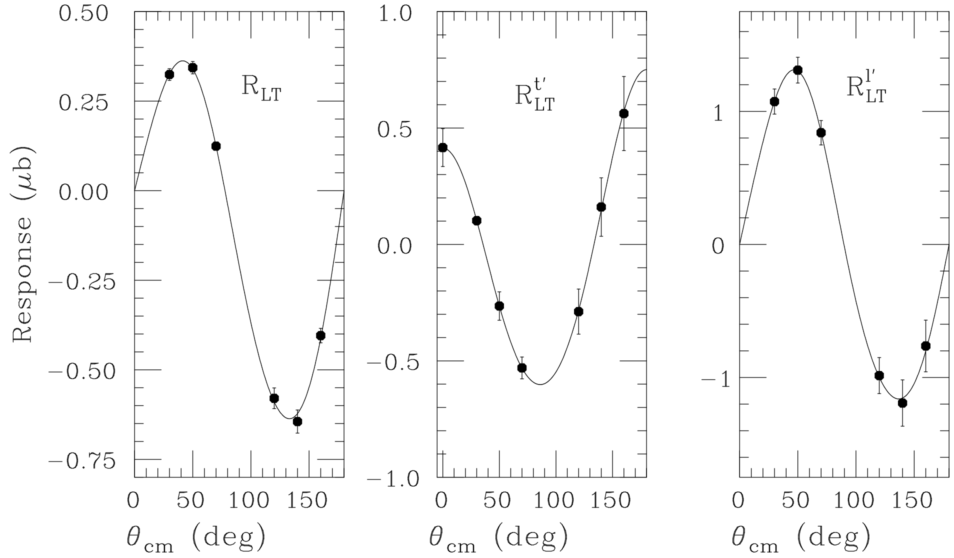

Figure 8. *Legendre polynomial fits of LT-type response functions. The error bar is the projected statistical uncertainty. The fit included an 8% systematic uncertainty on each point as well.*

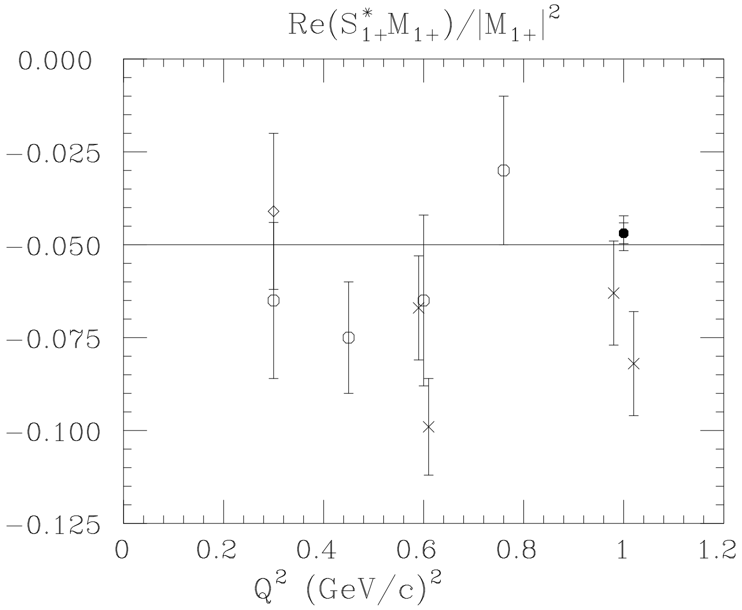

Figure 9. *The projected result of this experiment for* $\mathrm{Re}(S^*_{1+}M_{1+})$ *(solid symbol) compared to previous data.*[13][14] *The inner (outer) bar is the statistical (total) uncertainly.*

definition of the kinematics (Q^2, W etc.) for each event and uncertainties associated with parameters of the experimental apparatus (target thickness, analyzing power of the FPP etc.) The effects of these are somewhat different in parallel and non-parallel kinematics since, in parallel kinematics, each polarization component corresponds to a single response functions while in non-parallel kinematics two measurements must be combined to extract the response functions. However, the influence of certain systematics are minimized by keeping both the beam energy and scattered electron kinematics fixed throughout the course of the measurement; the proton momentum and angle are the only experimental quantities varied.

The Hall A spectrometer pair, along with the high quality beam at CEBAF, will provide superb definition of the event-by-event kinematics. A momentum resolution of 3×10^{-4} in both the incident and scattered electron energies and an angular resolution of 1.0 mrad will result a Q^2 resolution of 1.4–4.2$\times 10^{-3}$ GeV^2 and an invariant mass resolution of 0.8–2.7 MeV (depending on the particular kinematics). Of course, while for statistical reasons the data must be collected in considerably larger bins, the high resolution allows the center of each (large) bin to be precisely located. This is essential when two measurements must be combined to extract response functions. There are two relevant issues here: one is that, since each event carries with it a "weight" (the cross section for producing that event) then, to obtain the correctly weighted population of the phase space in a given measurement depends on being able to locate the (small) phase space bin for each event accurately. Secondly, the response function separation can only be meaningfully carried out over that region of phase space which is common between the two measurements. Although in the idealized case there is complete symmetry between measurements made on either side of $\vec{q}$, in practice this is not the case since, e.g., the variation of the cross section with electron scattering angle causes $\vec{q}$ to point away from its nominal direction in an asymmetric fashion. Thus, precise location of the phase space boundary is required for proper extraction of the response functions.

Monte-Carlo studies for each kinematics have been performed using the computer code MCEEP.[35] This code averages a physics model over the finite acceptances of the experimental apparatus and includes the effects of offsets and finite resolutions. Typical results are shown in Figures 10 and 11. In Figure 10 we show the cross-section-weighted sampling of invariant mass for the two measurements at $\theta_{cm} = 30°$. Figure 11 compares the population of the θ_{cm}-Q^2 plane for the measurement at $\theta_{cm} = 70°$.

The simulations we performed indicate that systematic uncertainties associated with kinematic definition can be kept below 5% in the extracted response functions although, as discussed above, we assumed 8% when performing the multipole analysis. Also note that the situation in pion production is somewhat less severe than in (e,e$'$p) from a nuclear system since, in the former case, one does not have the additional rapid variation due to the nuclear momentum distribution (further quantitative results can be found in the CEBAF CDR[36]).

Figure 12 shows the missing mass acceptance and resolution expected in the two extreme kinematics: $\theta_{cm} = 0$ and 160°. In all the Monte-Carlo studies we assumed that the momenta are known a factor of three worse than design goals, i.e., known to 3×10^{-4} and that angles were known only to 1 mrad. The resulting resolution is still excellent so that a cut on the pion peak greatly improves the signal-to-noise ratio. However, at the large CM angles, the missing mass acceptance no longer has the broad, flat region it did at 0°. Accurately reconstructing the missing mass is then also necessary to properly account for the acceptance variation.

The other main systematic effects result from the knowledge of the $\vec{p}$-^{12}C analyzing power and the electron beam polarization. All of the proton energies that occur in this experiment are < 800 MeV so that the extensive analyzing power data base from LAMPF, SIN and TRIUMF is applicable. A global fit to the entire data set[37] resulted

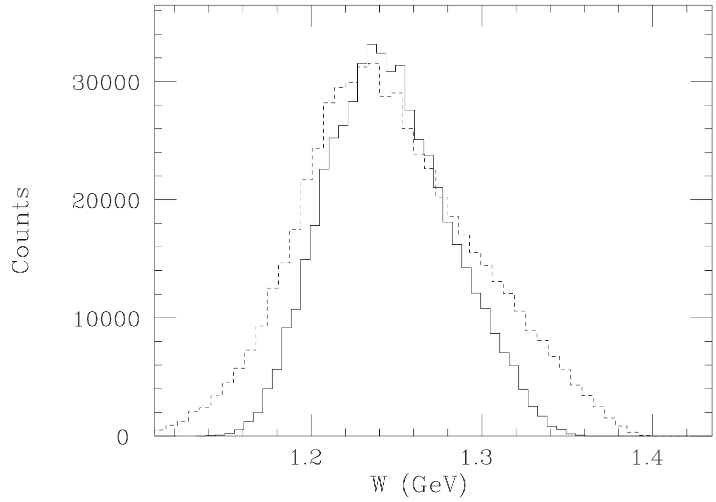

Figure 10. *Sampling of invariant mass for $\theta_{cm} = 30°$. Solid: $\phi = 0$, dashed: $\phi = 180°$. The distributions are weighted by the cross section.*

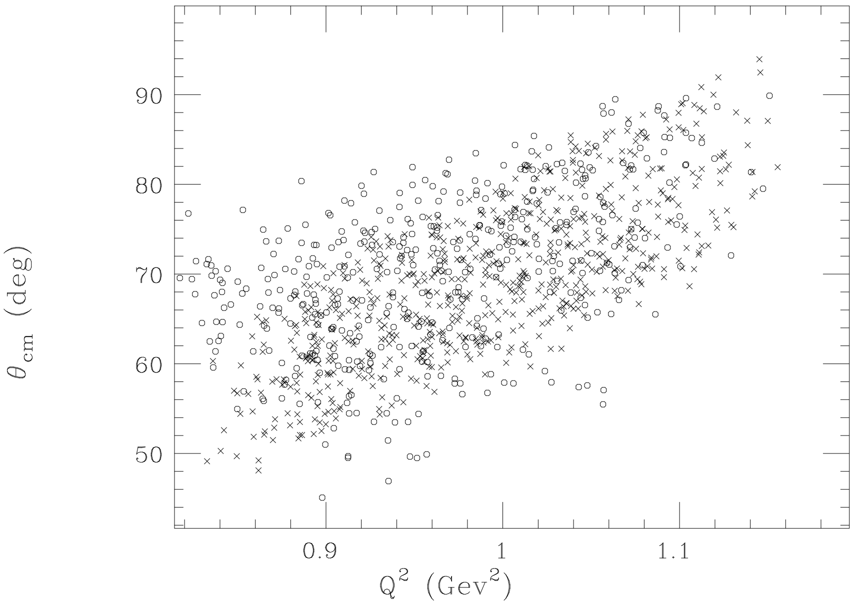

Figure 11. *Monte-Carlo population of the variables θ_{cm} and Q^2. The circles correspond to the measurement at $\theta_{cm} = +70°$ and the crosses to the measurement at $-70°$.*

in an uncertainty on $A_y(\theta)$ of only $\pm 2\%$. There is also overlap with the higher energy data from recent measurements at SATURNE.[38] The electron beam polarization will be measured with a standard Møller polarimeter and should be good to 3–5%.

4. Count Rate Estimates

In preparing the count rate estimates we assume the following:

- 15 cm liquid hydrogen target thickness: 1.1 g/cm^2
- 40% polarized electron beam current: 100μA

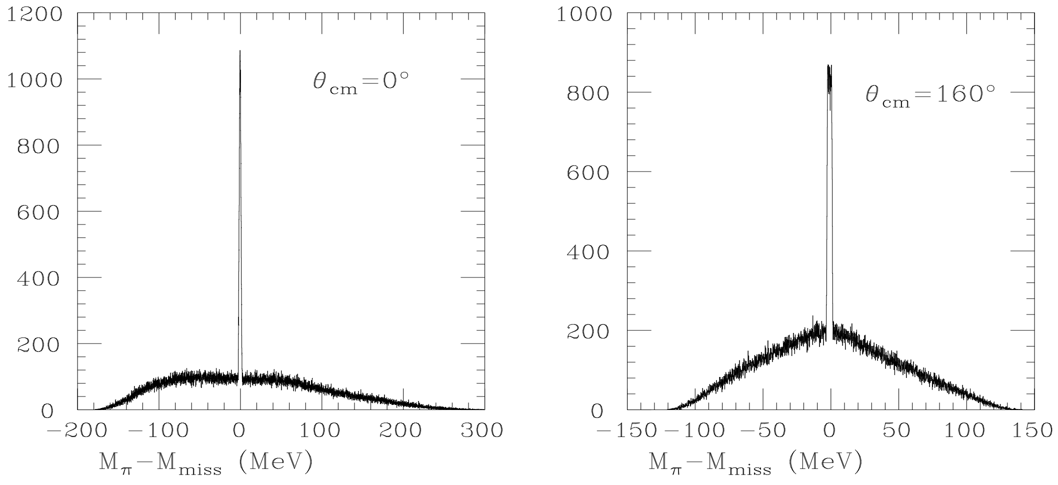

Figure 12. *Monte-Carlo calculation of missing mass acceptance at the two kinematic extremes (θ_{cm} = 0 and 160°). The narrow structure is the pion peak from the real coincidence events.*

- HRS^2 solid angle and momentum bite: 7 msr and 10%

The (e,e′) and (e,p) singles cross sections were calculated using the codes QFS and EPC from O'Connell and Lightbody.[39] The resulting rates are well within the capabilities of the Hall A detectors and data acquisition system. The (e,e′p) true coincidence rate was computed using the DL parameterization of the multipole amplitudes and folded over the experimental acceptances using the code MCEEP.[35] The signal-to-noise ratio, after applying a missing mass cut at the pion mass (see Figure 12), is always very favorable, never being less than 6:1. The rates are summarized in Table 3.

The statistical uncertainty of a polarization component at the focal plane is:

$$\Delta P_{fp} = \frac{\pi}{2} \frac{1}{\langle A_y \rangle} \sqrt{\frac{1}{\epsilon N}} \quad , \tag{15}$$

where N is the total number of events incident on the polarimeter and ϵ is the fraction that scatter usefully. The polarimeter efficiency and analyzing power were estimated using the parameterizations from LAMPF[37] and SATURNE.[38] Figure 13 shows the expected figure-of-merit ($= \epsilon A_y(\theta)^2$) for the FPP as a function of proton energy along with the energies of our proposed points. We found a reasonable compromise between precision in all the response functions and running time. In all cases, the precession of the $\hat{n}$ and $\hat{\ell}$ components of the polarization in the HRS magnets has been accounted for. The beam time request is summarized in Table 4 (a radiative correction factor of 1.3 has been included).

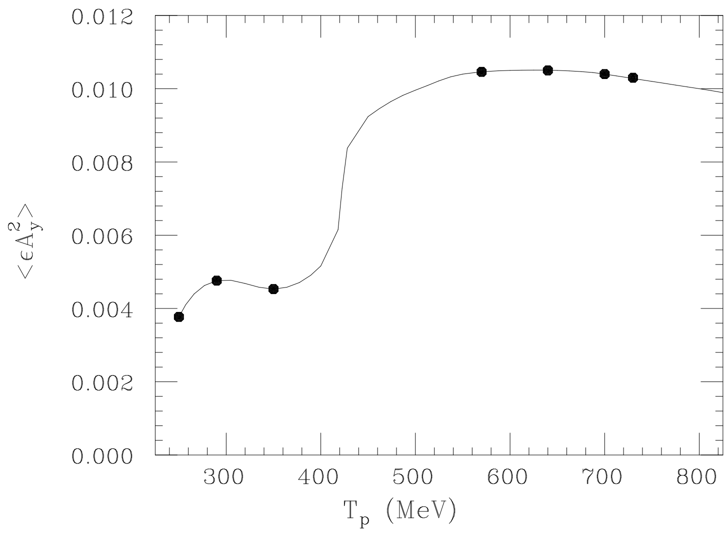

Figure 13. *The polarimeter figure-of-merit. Results are the angle-average for scattering angles in the FPP from 4 to 20° . The solid symbols denote the proton energies in this proposal.*

Summary

We propose to exploit the unique capabilities of Hall A, namely high precision kinematic definition and proton polarimetry, to study the $N \to \Delta$ transition. We expect to obtain a precise value for the Coulomb quadrupole amplitude at $Q^2 = 1.0$ GeV^2 by simultaneously determining 3 of the 4 response functions that contain the $\mathrm{Re}(S_{1+}^* M_{1+})$ interference term. We will determine several previously unmeasured response functions which contain both real and imaginary parts of interferences. By doing so, we will significantly test all the dynamical ingredients, resonant and non-resonant, in the elementary pion electroproduction process.

Counting Rates

R(e,e')= 5.5×10^4 s^{-1}

θ_{cm} (deg)	ϕ (deg)	R(e,p) (s^{-1})	$R_{accid.}$ (s^{-1})	R(e,e'p) (s^{-1})
0	—	2.2×10^5	24	226
30	0	2.4×10^5	26	147
30	180	1.9×10^5	21	265
50	0	2.7×10^5	30	108
50	180	1.8×10^5	20	284
70	0	2.9×10^5	32	82
70	180	1.7×10^5	19	260
120	0	3.5×10^5	39	36
120	180	1.8×10^5	20	82
140	0	3.6×10^5	40	29
140	180	2.1×10^5	23	42
160	0	3.4×10^5	37	22
160	180	2.4×10^5	26	26

Table 3. *Singles and coincidence counting rates. Note that the accidentals rates are for the* *full* *acceptance; a missing mass cut at the pion mass will reduce this by a factor of at least 10. A coincidence time resolution of 2ns was assumed.*

Beam Time Request

θ_{cm} (deg)	Counts desired	time (days)
0	1.3×10^7	1.0
30	9.7×10^7	3.5 ($\times$2)
50	9.2×10^7	3.5 ($\times$2)
70	7.9×10^7	3.5 ($\times$2)
120	2.8×10^7	3.5 ($\times$2)
140	1.6×10^7	3.5 ($\times$2)
160	1.1×10^7	3.5 ($\times$2)
		TOTAL: 43
		Angle changes, overhead: 2
		GRAND TOTAL: 45

Table 4. *Summary of beam time request. The numbers of counts for $\theta_{cm} \neq 0$ is the total for the measurements at $\phi = 0$ and $\phi = 180°$.*

References

[1] S.L. Glashow, Physica **96A**, 27 (1979).

[2] V. Vento, G. Baym and A.D. Jackson, Phys. Lett. **102B**, 97 (1981).

[3] P. Fishbane, J.S. McCarthy, J.V. Noble and J.S. Trefil, Phys. Rev. **D11**, 1338 (1975).

[4] L.M. Sehgal, Phys. Rev. **D10**, 1663 (1974).

[5] A. Abbas, J. Phys. **G15**, L195, (1989).

[6] J. Ashman *et al.*, Nucl. Phys. **B328**, 1 (1989).

[7] B. Adeva *et al.*, Phys. Lett. **B362**, 553 (1993).

[8] P.L. Anthony *et al.*, Phys. Rev. Lett. **71**, 959 (1993).

[9] A. Chodos and C.B. Thorn, Phys.Rev.**D12**, 2733 (1975);
S. Theberge, A.W. Thomas and G.A. Miller, Phys.Rev. **D22**, 2838 (1980); **D24**, 216 (1981).

[10] N.Isgur and G.Karl, Phys.Rev. **D18**, 4187 (1978); **D19** ,2653 (1979).

[11] N. Isgur, G. Karl and R. Koniuk, Phys. Rev. **D25**, 2394 (1982).

[12] J. Biénkowska, Z. Dziembowski and H.J. Weber, Phys. Rev. Lett. **59**, 624 (1987).

[13] W. Albrecht *et al.*, Nucl. Phys. **B25**, 1 (1970) and **B27**, 615 (1971);
J.C. Alder *et al.*, Nucl. Phys. **B46**, 573 (1972).

[14] R. Siddle *et al.*, Nucl. Phys. **B35**, 93, (1971).

[15] G. von Gehlen, *Threshold Pion Electro- and Photoproduction*, Universität Bonn report 2–80 (1970).

[16] R.C.E. Devenish and D.H. Lyth, Nucl. Phys. **B43**, 228 (1972).

[17] S.S. Gershtein and G.V. Dzhikiya, Sov. J. Nucl. Phys. **34**, 870 (1981).

[18] S.A. Gogilidze, Y.S.Surovtsev and F.G.Tkebuchava, Sov. J. Nucl. Phys. **45**, 1085 (1987).

[19] M. Warns, H. Schroeder, W. Pfeil and H. Rollnik, Z. Phys. **C45**, 627 (1990).

[20] J.G. Koerner, Z. Phys. **C33**, 529 (1987).

[21] CEBAF PR-89–037, V. Burkert and R. Minehart.

[22] CEBAF PR-89–042, V. Burkert and R. Minehart.

[23] CEBAF PR-91–023, V. Burkert, D. Crabb and R. Minehart.

[24] CEBAF PR-93–036, H. Weller, R. Chasteler, R. Minehart.

[25] A.S. Raskin and T.W Donnelly, Ann. Phys. **191**, 78 (1989).

[26] R.W. Lourie, Z. Phys. C. **50**, 345 (1991).

[27] R.W. Lourie, Nucl. Phys. **A509**, 653 (1990).

[28] C. Giusti and F.D. Pacati, Nucl. Phys. **A504**, 685 (1989).

[29] A. Picklesimer and J.W. Van Orden, Phys. Rev **C35**, 266 (1987).

[30] G.G. Ohlsen and P.W. Keaton Jr., Nucl. Inst. Meth. **109**, 41 (1973);
G.C. Salzman, C.K. Mitchell and G.G. Ohlsen, Nucl. Inst. Meth. **109**, 61 (1973).

[31] J.M. Laget, Nucl. Phys. **A481**, 765 (1988).

[32] G. v. Gehlen, Nucl. Phys. **B9**, 17 (1969).

[33] B. Boden and G. Kroesen, *CEBAF Summer Study*, 121 (1986).

[34] H.J. Weber, in *Progress in Nuclear Physics*, Eds. W.-Y. Pauchy Hwang *et al.*, Elsevier, (1991), pp. 206–221 and University of Virginia preprint UVa-INPP-90–5.

[35] P.E. Ulmer, computer code MCEEP (1991).

[36] CEBAF Conceptual Design Report (1990).

[37] M.W. McNaughton *et al.*, Nucl. Inst. Meth, **A241**, 435 (1985).

[38] B. Bonin *et al.*, Nucl. Inst. Meth. **A288**, 379 (1990).

[39] J.W. Lightbody Jr. and J.S. O'Connell, *Computers in Physics* (1988).